Abou khadrah and Bedeer *Egyptian Journal of Radiology and Nuclear Medicine* (2019) 50:6
https://doi.org/10.1186/s43055-019-0006-y

Egyptian Journal of Radiology and Nuclear Medicine

RESEARCH Open Access

A small hepatic nodule (≤2 cm) in cirrhotic liver: doTriphasic MRI and Diffusion-weighted image help in diagnosis

Rania Sobhy Abou khadrah[1*] and Asmaa Bedeer[2]

Abstract

Background: Diagnosis of a small hepatic focal lesion (≤ 2 cm) in a cirrhotic liver by MRI depending on its characteristic signal intensities at different sequences, contrast enhancement, and diffusion-weighted image (DWI). Liver nodules were divided into malignant or benign according to the combination of different imaging features such as contrast uptake pattern, presence of fat, necrosis, diffusion pattern, and ADC value. We study about hepatic nodules which are difficult to diagnose using triphasic CT study due to a small size which make a characteristic pattern of enhancement of these focal lesions confusing and inadequate. Triphasic MRI and DWI increase the accuracy of the diagnosis of small nodule ≤ 2 cm and help in better treatment and intervention. The purpose of the study is to clarify the role of triphasic MRI and diffusion in differentiating a small hepatic nodule less than 2 cm in cirrhotic liver.

Results: Out of 60 patients with 124 hepatic nodules, MRI findings revealed 40 cases with malignant nodules (66.7%), 12 cases with premalignant nodules (20%), and 8 cases with benign nodules (hemangioma) (13.3%).

Conclusion: Combined triphasic MRI and diffusion WI increase the accuracy of the diagnosis of small hepatic focal lesions in the cirrhotic liver which may be difficult to diagnose by other imaging modalities, and help in early management and intervention.

Keywords: Triphasic MRI, Diffusion, Cirrhosis, Nodules

Background

Liver cirrhosis occurs due to an irreversible renovation of the hepatic parenchyma with fibrosis and formation of different types of hepatocellular nodules. Predisposing causes of cirrhosis include hepatitis C virus followed by hepatitis B virus and alcohol consumption [1].

Cirrhosis-associated hepatocellular nodules occur due to the focal area of hepatocytes and stromal proliferation in response to liver injury leading to the formation of regenerative nodules. In regenerative nodules, some liver cells may undergo further atypical genomic changes which lead to hepatocyte dysplasia, and the nodules increase rapidly in size and cellularity and transformed into dysplastic nodules and lastly hepatocellular carcinoma (HCC) [2].

Cirrhotic liver nodules were classified into regenerative, dysplastic, and neoplastic nodules [3].

Dysplastic or neoplastic nodules are composed of hepatocytes with atypia caused by genetic alteration. Neoplastic nodules were divided into adenoma, dysplastic foci, dysplastic nodules, and HCC [4].

Early detection and differentiation of small hepatic nodules ≤ 2 cm in the cirrhotic liver is a common problem in the diagnosis of small nodules by ultrasound or triphasic CT as many of them show atypical behavior in triphasic CT and confusing ultrasound imaging [5, 6].

Triphasic MRI study and diffusion WI help in the early detection of these small-sized nodules and help in differentiating whether it is benign or malignant, and this lead to the early intervention and better prognosis [7].

* Correspondence: rotinia2009@gmail.com
[1]Radiology Department, Faculty of Medicine, Tanta University Hospital, Tanta University, 15 Ebn Elphared Street, Tanta, Gharbia Governorate 31511, Egypt
Full list of author information is available at the end of the article

Material and methods

Population

The current study started from February 2016 to March 2018. It was carried out on 16 cirrhotic liver patients with nodules ≤ 2 cm referred to a radiology department from internal medicine and oncology units. Twenty out of 60 patients underwent ultrasonography (US) before the MR examination while the remaining 40 patients underwent both CT and US.

The 60 patients included 48 males and 12 females, and their age ranged from 43 to 69 years.

Methods

Inclusion criteria

The following are the inclusion criteria:

- Cirrhotic liver patients of any etiology with elevated liver enzymes and alpha-fetoprotein (AFP) above 10 ng/ml
- Had focal nodule/nodules ≤ 2 cm detected by US and/or MSCT with insufficient or confusing diagnostic criteria as a typical pattern of enhancement on triphasic CT (nodule did not show typical features in initial imaging).

Exclusion criteria

The following are the exclusion criteria:

- Cirrhotic liver patients with no hepatocellular nodules or large nodule or mass > 2 cm
- Cirrhotic liver patients with a nodule/nodules ≤ 2 cm but showed typical diagnostic criteria by triphasic CT study
- Patients with acute renal insufficiency to avoid hepatorenal syndrome with IV Gd-DTPA injection

A. A full history details including age, sex, and clinical presentation about symptom and signs as jaundice, pallor, edema, ascites, and cachexia, a clinical assessment was done by a physician with 5 years of experience.
B. Laboratory investigations consist of liver and renal function tests and alpha-fetoprotein (AFP).
C. Preliminary ultrasound or triphasic CT study was done for all patients for the detection of a typical nodule/nodules (a nodule did not show typical features in initial imaging) which needs further assessment by MRI.
D. Abdominal MRI: conventional MRI, post-Gd-DTPA, and triphasic MRI were performed on (1.5 T) magnet units (CIGNA Healthcare, USA), and a phased array coil was used to cover the whole liver. Patients were fasting for at least 6 h, and no medications were given before the examination.

MRI protocol is done with the followings sequences:

- T1-weighted (T1W) images: repetition time (TR) = 10 ms, echo time (TE) = 4.58 ms, matrix 179 × 320, slice thickness 7–8 mm, slice gap 1–2 mm, and FOV 355 mm.
- T2-weighted (T2W) images with single-shot free breathing: TR ≥ 445 ms, TE = 26–28 ms, matrix size 180–200 × 240, slice thickness 7–8 mm, slice gap 1–2 mm, and FOV 365 mm.
- T2 spectral attenuated inversion recovery (SPAIR) with fat suppression sequence: TR ≥ 400 ms, TE = 70 ms, matrix size 204 × 384, slice thickness 7–8 mm, slice gap 1–2 mm, and FOV 365 mm.
- Breath-hold heavy T2WI was done with half-Fourier acquisition turbo-spin echo (HASTE) TE 150 ms, a matrix 320 × 179, slice thickness 4 mm, slice gap 1 mm, and acquisition time 18 s.
- Both in-phase and out-phase gradient echo sequences (dual/FFE) were used with the parameter of the in-phase: TR = 75–100 ms, TE = 4.6 ms and 2.3 ms for out phase, matrix 143 × 240, slice thickness 7–8 mm, slice gap 0 mm, and FOV 345 mm.

A triphasic study was performed after an injection of a bolus 0.1 mmol/kg of the body weight of Gd-DTPA with a rate of 2 ml/s, followed by 20 ml of sterile 0.9% saline solution for flushing through the antecubital vein. The injection of gadolinium and saline solutions was done manually. Triphasic imaging using the T1-weighted high-resolution isotropic volume examination (T1 THRIVE) technique was performed dynamically: first, the arterial phase (16–20 s), followed by porto-venous phase (45–60 s), and lastly, the delayed equilibrium phase (3–5 min) after the administration of the gadolinium.

D. Diffusion WI: a single shot respiratory-triggered fat-suppressed DW imaging was performed in the axial plane using a diffusion gradient of b value 1000 s/mm^2 to increase the sensitivity to cellular packing. A repetition time (TR) of ≥ 1880 ms, an echo time (TE) of 70 ms, a matrix of 256 × 256, a slice thickness of 7–8 mm, a slice gap of 1–2 mm, and a scan time of 3–4 mm.

E. Histopathological analysis: CT-guided procedures were performed on a 64-slice MDCT (GE Healthcare). The MDCT parameters for guiding liver biopsy and immediate follow-up scanning were set as follows: 120–140 kVp, 80–200 mAs, and slice thickness 5.0–7.5 mm. Iodinated contrast media administered during the procedure when nodules were not detected by the operator for localization, a combined core biopsy, and fine needle aspiration FNA is a standard protocol. A semi-automated 17-gauge introducer–18-gauge coaxial biopsy needle system was used. An operator used local anesthesia at the puncture site; a 17-gauge needle with

Table 1 Qualitative analysis of 124 hepatic nodules by MRI and diffusion WI

	Reader 1		DWI	*p* value	Reader 2		DWI	*p* value
	Pre-contrast	Post-contrast			Pre-contrast	Post-contrast		
TP(*n*)	95	100	100		93	102	103	
TN(*n*)	20	18	20		22	19	16	
FP(*N*)	4	5	2		4	2	3	
FN(*N*)	5	3	2		5	1	2	
Sensitivity (%)	94.5	93.5	96.3	0.89	91.5	89.4	97.4	1.02
Specificity (%)	92.4	92.6	93.8		92.5	88.9	94.3	
PPV (%)	95.7	95.3	97.2		95.6	93.8	96.4	
NPV (%)	90.1	89.3	86.8		88.9	84.3	84.7	

an inner stylet was introduced into the target lesion. When the location of the needle was confirmed, the inner stylet was removed, and three to five FNAs with a 22-gauge needle and at least three core biopsies with an 18-gauge core needle were obtained. The sample size of core biopsy is usually 0.8–1 mm thick and 10–15 mm long. All core biopsy samples were put into formaline 10/100 and sent for cytology. FNA samples (smeared or slider) were stabilized with 95% ethanol and sent for cytology.

Imaging evaluation

Qualitative analysis of hepatic nodule/nodules by two readers who were blinded to each other (observer 1 with 5 years of experience and observer 2 with 3 years of experience) in writing abdominal MRI, both readers were blind about the history and laboratory investigation. They used the Advantage Window Workstation (GM Medical Systems) for the evaluation of the pre-contrast T1 and T2WI for the site, size, number of lesions, and signal intensity and then evaluate post-contrast study for different phases (arterial, portal, venous, and delayed), in-phase and out-phase for lipid content, lastly DWI and ADC map by putting an oval region of interest (ROI) over the lesion. Multiple ADC values were measured, and the average was calculated. The results were matched with laboratory and histopathological findings in all patients except 8 cases of hemangioma where the final diagnosis assessed by AFP and follow up for a change of size or signal intensity of the nodule.

Inter- and intraobserver quantitative evaluation of all cases as the two readers agreed on the finding of the signal intensity and pattern of enhancement of the lesions, the observer was blinded about the histopathology with no significant difference between both readers, p value > 0.05 as shown in Table 1; intraobserver evaluation was done by both readers after 2 months.

Statistical analysis

Analysis of demographic, clinical, radiological, and pathological data of the patients was done with an emphasis on the role of triphasic MRI and diffusion; variables were expressed as a mean ± standard deviation to measure the degree of dispersion of data around the stander data; a chi-squared test was used for the variable to assess the presence of significant difference; the receiver operating characteristic curve was constructed and its parameters (sensitivity, specificity, positive predictive value, and negative predictive value), as well as the accuracy, were estimated; SPSS Statistical Software version 22 was used with p value analysis was done; p value less than 0.05 was considered statistically significant. Optimal ADC threshold values for nodule discrimination were assessed by means of receiver operating characteristic (ROC) curve analysis with the calculation of cutoff value, and corresponding sensitivities and specificities were calculated. Statistical qualitative analysis of 124 hepatic nodules was performed with Medcalc v.9 (Medcalc Software, Belgium) to assess the interobserver agreement in assigning a confidence level to the lesion status. Cohen's kappa suggested the Kappa result be interpreted as follows: values ≤ 0 indicates no agreement, 0.01–0.20 none to slight, 0.21–0.40 fair, 0.41–0.60 moderate, 0.61–0.80 substantial, and 0.81–1.00 almost perfect agreement.

Results

This study included 60 patients, 48 males (80%) and 12 females (20%). The patient's age ranged between 43 and 69 years, mean age of 55.67 years as shown in Table 2.

All patients in our study had biopsied except for 8 cases with hemangioma Which we depended in its final diagnosis upon follow-up by AFP and repeated MRI every 3 months

Table 2 Age distribution in 60 patients and their percentage

Age (years)	*N* (60)	
	N	%
40 < 50	12	20
50 < 60	32	53.3
60 < 70	16	26.7
Total	60	100

Table 3 Accuracy of MRI finding in our study

Diagnosis	Number/percentage of MR cases	Number/percentage of the biopsy cases
HCC nodules	40 (66.7%)	40 (76.9%)
High-grade dysplastic nodules	8 (13.3%)	8 (15.4%)
Low-grade dysplastic nodules	4 (%)	
Regeneration nodules		4 (7.7%)
Hemangioma	8 (13.3%)	
Total	60 (100%)	52 (100%)
Accuracy (%)	93.3	100
p value	0.058	

to detect no change in size, signal intensity, and pattern of enhancement.

Histopathological examination of 52/60 cases revealed 40 cases had confirmed to be malignant nodules (76.9%), 8 cases with premalignant nodules (15.4%), and 4 cases with regeneration nodules (7.7%).

Histopathological examination of 52/60 patients who had biopsied were correlated and confirmed with MR finding as we found that out of 52 patients, 40 patients had confirmed to have malignant nodules with an accuracy of 100%, while 8 cases with high-grade dysplastic nodules had confirmed also histopathologically to be premalignant on biopsy with an accuracy of MR 100% and 4 cases with a low-grade dysplastic nodule on MR had confirmed to be regeneration nodules on biopsy with an accuracy of MR 48/52 (92.3%).

The included 60 patients were divided according to their final diagnosis with triphasic MRI and diffusion with a correlation to histopathological analysis as shown in Table 3.

The 60 patients included in this study had 124 primary hepatic focal lesions. They were divided according to the MRI and pathological correlation as shown in Table 4.

The anatomical distribution of the 124 primary hepatic nodules by MRI was as shown in Table 5.

The included hepatic focal nodules were divided as follows:

1. Group A (HCC nodules): There were 40 cases with 72 primary hepatic nodules; their laboratory tumor marker investigation (AFP) ranged between 43 and 2000 ng/ml with an average of 258.58 ng/ml.

Table 4 Division of 124 hepatic nodules by MRI and pathological correlation

The pathological lesions	Number of lesions	Percentage
HCCs	72	58.1
High-grade dysplastic nodules	28	22.6
Low-grade dysplastic nodules	16	12.9
Regenerative nodules		
Hemangioma	8	6.5
Total	124	100

Table 5 Anatomical distribution of 124 hepatic nodules

The site of the pathological lesions	Number of lesions	Percentage
Rt hepatic lobe	52	41.9
Lt hepatic lobe	16	12.9
Entire hepatic lobes	56	12.9
Total	124	100

According to the MR findings, group A (HCC nodules) were divided into 3 subgroups (Table 6, Figs. 1, 2, and 3).

The MRI signal intensities and the ADC values are as follows:

1. Group A (HCC nodules): There were 40 cases with 72 nodules with low SI in T1WI, high SI in T2 SPAIR, and isointense in out-phase and low signal in in-phase with 32 nodules showing restricted diffusion, and 8 nodules were partially restricted with ADC value of $0.94 \times 10^{-3} \pm 1.20 \times 10^{-3}$ with a mean value of $1.040 \times 10^{-3} \pm 0.20\ mm^2/s$.
2. Group B (dysplastic nodules): There were 12 cases with 44 primary hepatic focal lesions (16 nodules with low-grade dysplasia and 28 nodules with high-grade dysplasia). Their laboratory tumor marker investigation (AFP) ranged between 13 and 54 ng/ml with an average of 26 ng/ml. The triphasic MRI findings were as follows:

(a) The high-grade dysplastic nodules (28): nodules were a hyperintense signal in T1, T2, and SPAIR, and all cases showed no restriction in DWI and their pattern of enhancement were 28 nodules that have faint contrast uptake in the arterial phase and more enhancement in portal phase and delayed phase as in Fig. 4.
(b) The low-grade dysplastic nodules (16) showed the same SI as high-grade nodules in all sequences and had no enchantment in the arterial phase and appeared isointense in portal phases with no washout.

ADC value of (group B) dysplastic nodules was $0.9x10^{-3} \pm 1.3 \times 10^{-3}$ mm/s with a mean value of $1.095 \pm 0.0108 \times 10^{-3}$.

Table 6 Division of group A nodules according to MRI

MR diagnosis	Number of cases	Percentage
Well differentiated HCCs	28	70
Complicated HCCs	8	20
Multicentric HCCs	4	10
Total	40	100

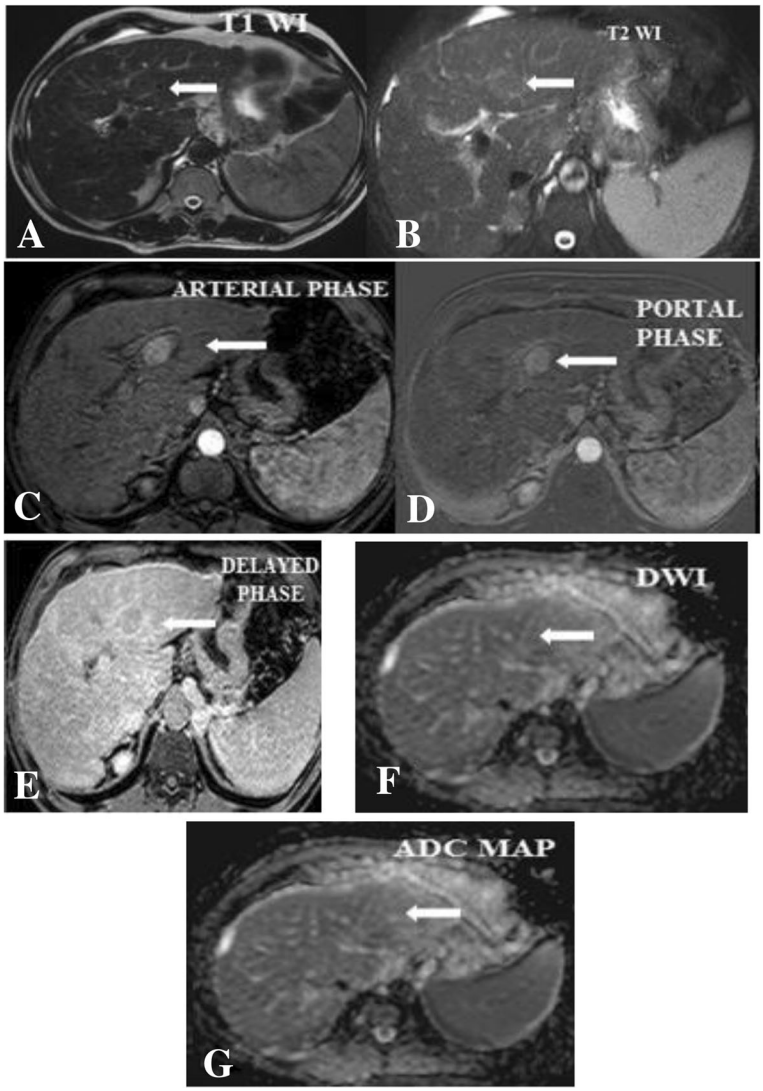

Fig. 1 A 60-year-old male patient post-transarterial chemoembolization. **a** An axial unenhanced T1W image showed newly appeared in the right lobe segment IVA focal lesion of isointense signal (arrow). **b** An axial T2W image showed a lesion of slight high signal (arrow). **c** An axial post-contrast arterial phase shows homogenous contrast enhancement (arrow). **d**, **e** An axial portal and the delayed gadolinium-enhanced image showed gradual contrast washout (arrow). **f**, **g** DWI shows the lesion to be restricted, and ADC MAP showed the lesion of low signal intensity with ADC value of 0.9 × 10−3mm2/s. Suggested MR diagnosis: hepatocellular carcinoma. Biopsy results: hepatocellular carcinoma

3. Group C (regeneration nodules): There were 4 cases with 16 regenerating nodules. Their clinical laboratory tumor marker investigation (AFP) ranged between 15 and 25 ng/ml.

The MR findings and ADC value in group C were high SI in T1WI and isointense signals in T2, SPAIR, and in-phase sequences, and all showed no restriction in DWI with ADC values of $1.23x10^{-3} \pm 0.17 \times 10^{-3}$ mm/s; the range was $1.10 \times 10^{-3} \pm 1.5 \times 10^{-3}$ and showed isointense signals in all phases of triphasic MRI study with no washout in the delayed phase, as seen in Fig. 5.

There were four falsely diagnosed lesions such as low-grade dysplastic nodules by MRI. However, the biopsy revealed them to be regeneration nodules. On dynamic MRI, the four lesions showed the same findings as the regeneration nodules, but they were hyperintense on T1WIs and isointense on T2 and SPAIR WIs. There was no signal drop in the opposed-phase images as compared to the in-phase images denoting no intracellular fat inside these nodules, and lesions were not restricted in the DWIs.

Group D hemangioma (8 cases): The triphasic MRI showed enhancement in the delayed phase only and showed no restriction in DWI with ADC value of $1.77 \times 10^{-3} \pm 0.35$;

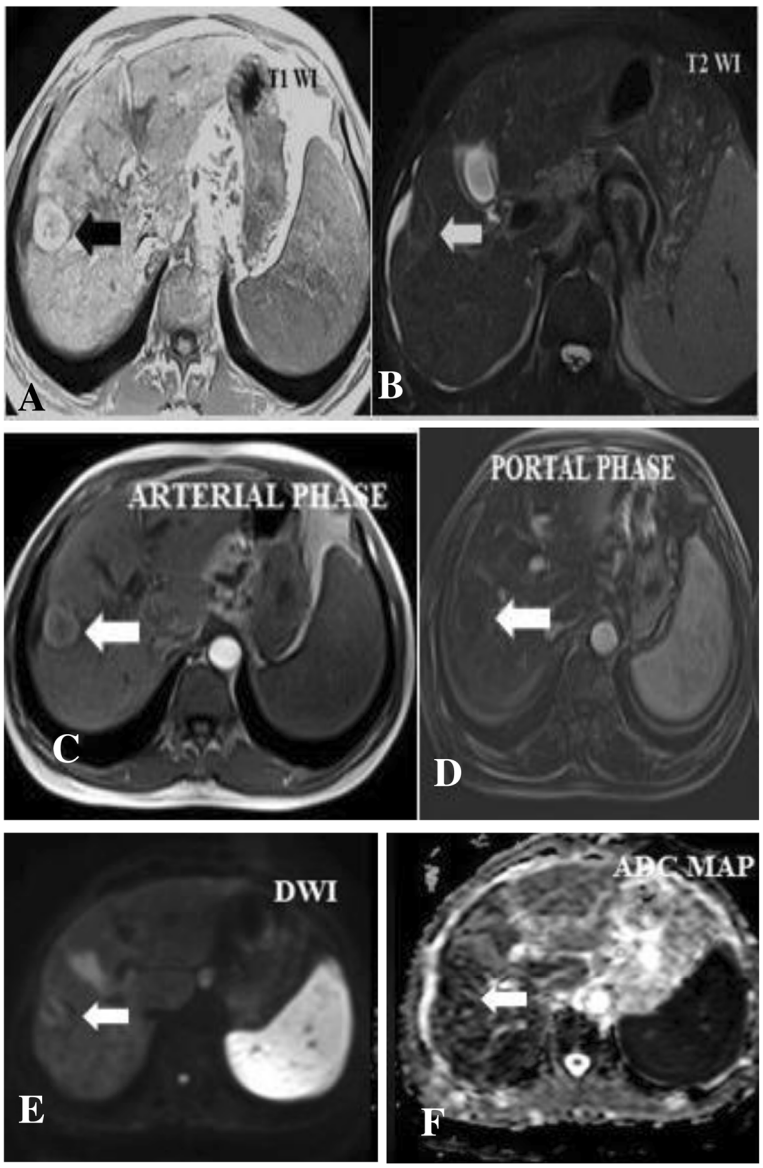

Fig. 2 A 59-year-old female presented with right hypocondrial pain. **a** An axial unenhanced T1W image shows right lobe segment V focal lesion measuring 2 cm of isointense signal (arrow). **b** An axial T2W image showed a lesion of hyperintense signal (arrow). **c** An axial post-contrast arterial phase image shows homogeneous contrast enhancement (arrow). **d**, **e** An axial portal and the delayed post-contrast images show contrast washout (arrow). **f** DWI shows the lesion to be partially restricted (arrow). With ADC value of 0.9 × 10−3mm2/s. Suggested MR diagnosis: HCC nodule. Biopsy results: HCC nodule

the range was $2.12 \times 10^{-3} \pm 1.42 \times 10^{-3}$ mm/s as seen in Fig. 6.

Diffusion and ADC values of all hepatic nodules included in our study are shown in Table 7.

ADC values had neither significant differences between the different type of malignant nodules (HCCs and dysplastic nodules) nor between different types of benign nodules (regenerative and hemangioma) but had significant value in discrimination between malignant and benign nodules. Our measurements for ADC values showed that ADCs of malignant lesions were significantly lower than those of benign lesions (p 0.001). There was a significant overlap between benign and malignant nodules, and the area under the curve for malignancy was 0.88 (sensitivity 88%, specificity 85%), using a cut-off of 1.22×10^{-3} mm^2/s. No significant difference was found between the ROIs of different characteristics of Table 8 and Fig. 7.

MRI and diffusion, sensitivity, specificity, and accuracy are shown in Table 9.

We tried to put a schematic diagram for reading the MRI in case of small nodules ≤ 2 cm as shown in Fig. 8.

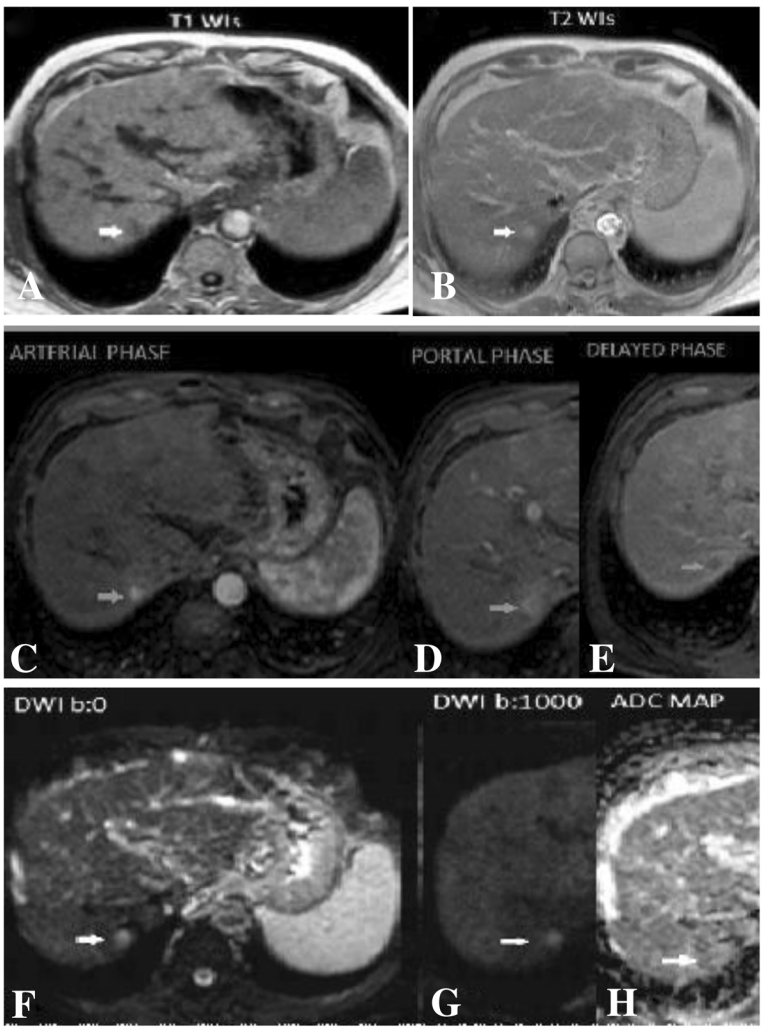

Fig. 3 A male patient aged 64 years old presented with lower limb edema. **a** An axial unenhanced T1WI image shows a lesion in the right hepatic lobe segment VII of low SI (arrow). **b** An axial T2WI shows a lesion of mildly increased SI (arrow). **c** An axial post-contrast arterial phase image shows intense enhancement of lesion, typical HCC (arrow). **d** An axial portal phase shows washout of the lesion. **e** An axial delayed image shows washout of the lesion with capsular enhancement (arrow). **f**, **g** DWI shows the lesion to be of increased SI owing to restricted diffusion (arrow). **h** An axial ADC map shows the lesion to be of decreased SI (arrow). Suggested MRI diagnosis: HCC nodule. Biopsy results: well-differentiated HCC

Discussion

Cirrhosis is a pathological process characterized by a continuous diffuse process of fibrosis and parenchymal distortion and an occurrence of different types of nodules either benign regenerative nodules, premalignant dysplastic nodules, or malignant hepatocellular nodules (HCC). The incidence of malignant nodules is expected to increase mainly due to the widespread hepatitis B and C infection. HCC nodules are the fifth most common malignancy in the world [8].

MRI nowadays is considered the most accurate imaging modality for the detection of cirrhosis and its complications. Short-time sequences, better soft tissue resolution, and Triphasic contrast examinations have become a basic component of abdominal imaging [9].

DWI, in addition, helps in a better differentiation of benign and malignant nodules [10].

In our work, the study population included 60 patients with a male predominance (48/60) of 80%. The sixth decade group was the most affected group (28/60) 46.7% followed by the seventh decade group (24/60) 40%.

By MRI, out of 60 patients, most types of nodules were HCCs 40/60 (66.7%). These findings matched with Glenn et al. whose study population included 71 patients (42 males, 29 females) with 65 HCC cases and Rieko et al. whose study population included 58 patients (39 males,19 females) with 40 HCC cases [11, 12]. In this study, group A HCC nodules (72/124) (58.1%) were hypointense on T1WIs and hyperintense on T2WIs and SPAIR; this signal pattern is typically the characteristic

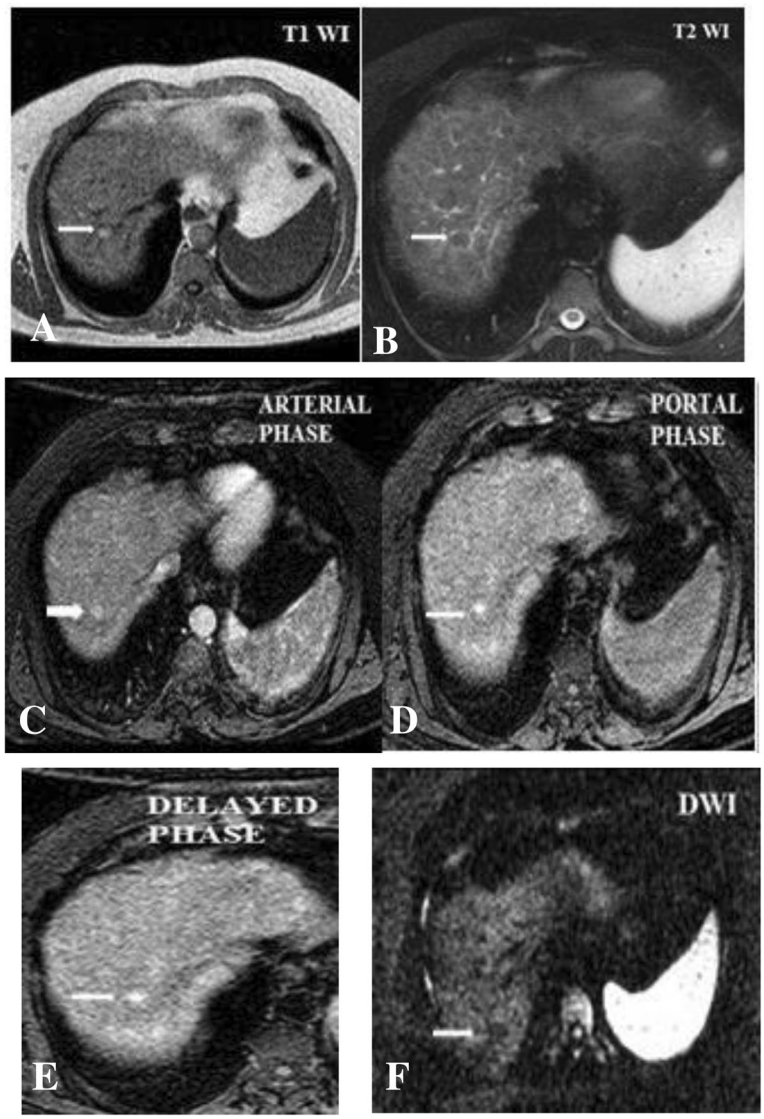

Fig. 4 A 54-year-old male presented with loss of appetite. **a** An axial unenhanced T1W image shows the right lobe segment IV focal lesion of high signal intensity (arrow). **b** An axial T2W image shows a lesion of low signal intensity (arrow). **c** An axial post-contrast arterial phase image showed homogeneous contrast uptake (arrow). **d**, **e** An axial portal and delayed images showed persistent contrast enhancement (arrow). **f** DWI shows the lesion to be of low signal due to non-restricted diffusion (arrow) with an ADC value of 0.7×10^{-3} mm^2/s. Suggested MR diagnosis: dysplastic nodule. Biopsy results: high-grade dysplastic nodule

for well-differentiated HCC nodules. These findings were also noted by Gaurav et al. and also Glenn et al. who reported that 94% of their 47 HCC nodule were hyperintense on T2WI [11, 13].

On the contrary, Van et al. published that the signal intensity of malignant nodules may be various on T2WIs and HCC nodules may be of similar signal or even low SI relative to the surrounding liver on Fat Sat T2WIs [14].

In our triphasic study, 64 out of 72 nodules (88.8%) of the group A nodules displayed the typical pattern of enhancement of malignant nodule as it showed rapid arterial enhancement and rapid contrast washout in the portal and delayed phases. These findings were similar to Robert et al., Jonathon et al., and Gaurav et al. who stated that this pattern of enhancement due to hypervascularity and they considered this pattern was essential characteristic features for HCC as the tumor recruits unpaired arteries and sinusoidal capillaries with resultant avid arterial enhancement [7, 13, 15].

Our study proved that all 28/124 were high-grade dysplastic nodules which showed hyperintense in T1WIs, T2WIs, and SPAIR. However, the 8/124 nodules of low-grade dysplastic nodules were also hyperintense

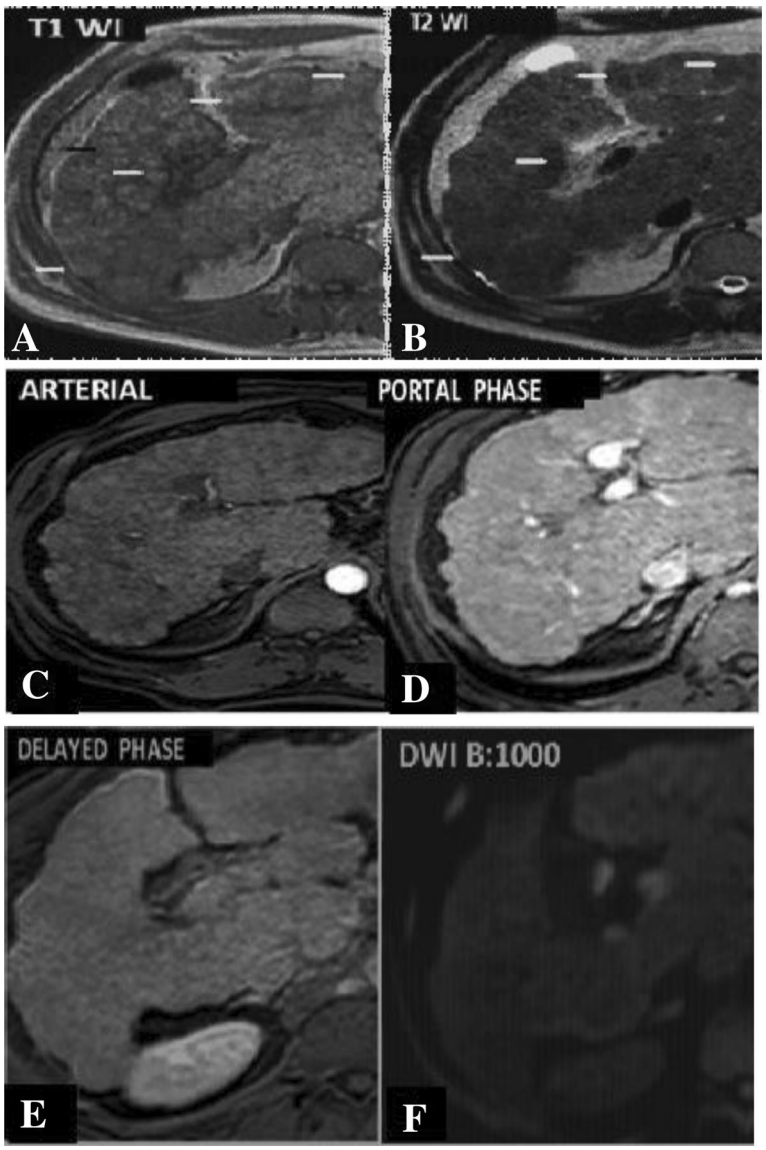

Fig. 5 A male patient aged 63 years old presented with tender abdomen who underwent ultrasonography and revealed several small nodules and referred to the MRI unit for further evaluation. **a** An axial unenhanced T1WI shows multiple nodules of isointense signal similar to liver parenchyma. **b** An axial T2WI shows the lesion to be of low SI. **c** An axial post-contrast arterial phase image shows the lesion to be isointense. **d**, **e** An axial portal and delayed post-contrast image shows the lesions were also isointense with no contrast uptake. **f** DWI shows the lesions were isointense owing to free diffusion. Suggested MRI diagnosis: multiple regeneration nodules. Biopsy results: confirmed regeneration nodules

in T1WI, but isointense in T2WI and SPAIR sequences. This data was also stated by Gaurav et al. and Tatsuyuki et al., who reported that T1WI dysplastic nodules characteristically demonstrate high SI which may be related to the deposition of copper, glycogen, protein, or lipid. In T2WI, most of the dysplastic nodules are usually isointense or low intensity. On the other hand, Jonathon et al. stated that dysplastic nodules may have different MR appearance, but in rare cases, they appeared hyperintense in T2WIs and STIR [7, 13, 16].

In our study, there was no significant difference between the two types of dysplastic nodules in their signal intensity on T1 and T2WIs, but Robert et al. reported that the high-grade dysplastic nodules had a slightly high signal intensity on T2-weighted images. In this case, the differentiation between HCC and the high-grade dysplastic nodule may be difficult even by pathology [15].

In our triphasic MRI study, the 28 nodules of high-grade dysplasia displayed subtle arterial enhancement. However, they became more intense in the subsequent portal and delayed phases more than the liver parenchyma. On the other hand, the 8 low-grade dysplastic nodules were similar to the liver parenchyma in all phases of the dynamic study.

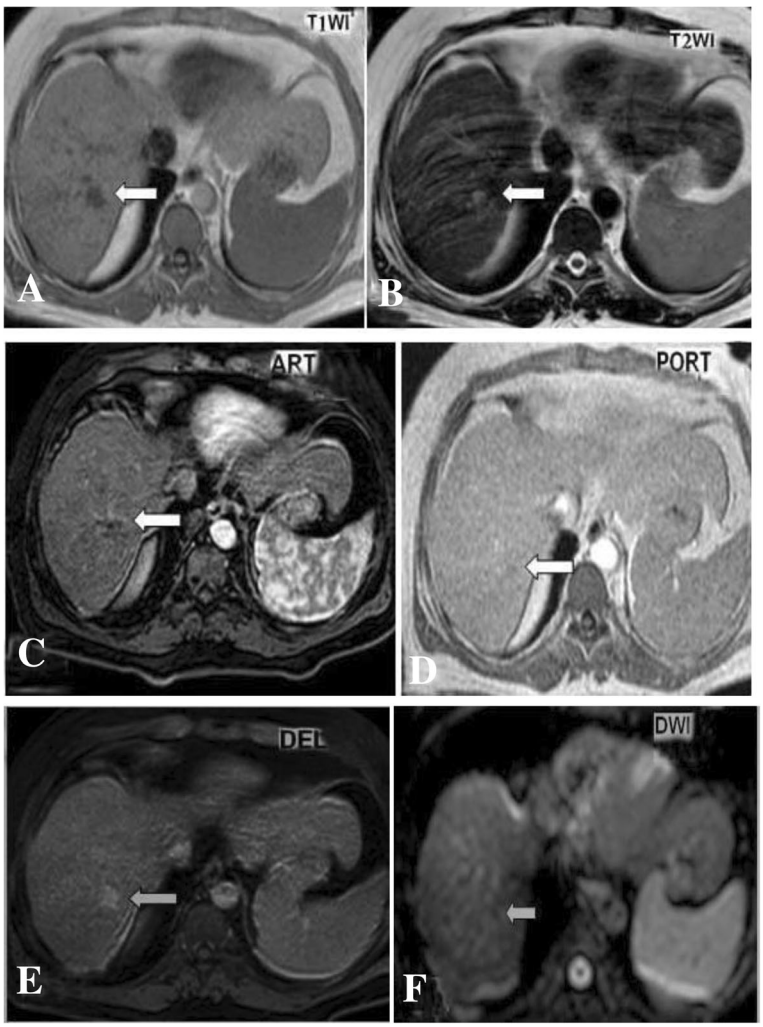

Fig. 6 A 56-year-old male had cirrhotic liver and right hepatic lobe focal lesion with an atypical pattern of enhancement on triphasic CT study. **a** An axial unenhanced T1W image shows the right hepatic lobe segment VII focal lesion of hypointense signal (arrow). **b** An axial T2W image shows the lesion of hyperintense signal (arrow). **c** An axial post-contrast arterial phase image shows hypoenhancement of the lesion (arrow). **d**, **e** An axial and delayed image shows contrast uptake without washout or enhancing capsule (arrow). **f** DWI of the lesion had low signal intensity (non-restricted diffusion) (arrow) with ADC value of 1.5×10^{-3} mm^2/s. Suggested MRI diagnosis: right hepatic lobe hemangioma

These findings were also noticed by Jonathon et al. Tatsuyuki et al. and Gaurav et al. who reported that as regards to the blood supply, the high-grade dysplastic nodules appear of low vascularity in the arterial phase with dominantly portal and venous blood supply, so they become more enhanced at portal and delayed phases with no contrast washout. The increased arterial vascularity was seen in a small number of high-grade dysplastic nodules that receive blood supply from the hepatic artery, and this may be confusing with HCC nodules during hepatocarcinogenesis. On the other hand, low-grade dysplastic nodules are normally supplied by the portal vein and therefore are similar to the liver parenchyma in all phases of triphasic contrast study [7, 13, 16].

Robert et al. reported that the regenerative nodules showed changeable signals on T1-weighted images. On the T2-weighted MRI, they were isointense to

Table 7 Diffusion and ADC value of hepatic nodules

	HCC nodules	Dysplastic nodules	Regenerating nodules	Benign nodules (hemangioma)	*p* value
Mean ADC ± SD	$1.040 \times 10^{-3} \pm 0.20 \times 10^{-3}$	$1.095 \pm 0.0108 \times 10^{-3}$	$1.23 \times 10^{3} \pm 0.17 \times 10^{-3}$	$1.77 \times 10^{-3} \pm 0.35 \times 10^{-3}$	0.001
Range of ADC value	0.94×10^{-3}–1.20×10^{-3}	0.9×10^{-3}–1.3×10^{-3}	1.10×10^{-3}–1.5×10^{-3}	2.12×10^{-3}–1.42×10^{-3}	

Table 8 Area under the curve (AUC) for ADC values and its cutoff value

	Cutoff	AUC	Sensitivity	Specificity	PPV	NPV	Accuracy
ADC value	1.22	0.88	88	85	92	77	87

Table 9 MRI and diffusion sensitivity, specificity, and overall accuracy

	Accuracy	Sensitivity	Specificity	PPV	NPV
MRI and diffusion	93.3	92.8	71.4	86.6	83.33

PV positive predictive value, NPV negative predictive value

hypointense but were almost never hyperintense [15]. In our study, group C, 16 regenerative nodules (13%) from 124 studied nodules showed high SI on T1WIs and isointense on T2WIs and SPAIR sequences. Since MRI signals of the regenerative nodules were variable, we cannot only rely on T1 and T2WIs to diagnose them [15].

In our triphasic study, group C regenerative nodules (16 nodules) were similar to the liver parenchyma with no evidence of arterial enhancement or washout owing to a large blood supply from the portal vein and minimal contribution from the hepatic artery. These findings were also found in the publication issued by Seale et al. stating that most of the regenerative nodules were enhanced as the liver parenchyma or show very faint enhancement as uptake, and excretion of gadolinium (DTPA) by these nodules is similar to normal liver tissue. Consequently, after contrast injection, all regenerative nodules have an equivalent intensity to the liver parenchyma which gave the liver homogenous appearance [17].

In our study, in group D, 8 cases of hemangiomas (8 nodules/124) (6.5%) were characteristically hypointense

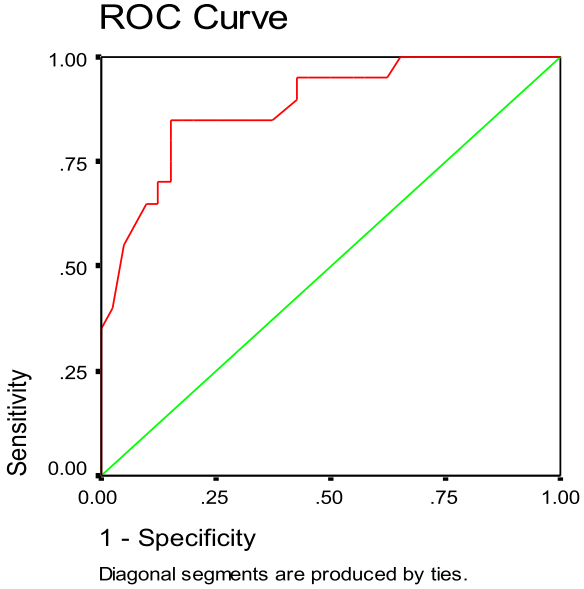

Fig. 7 ROC curve for ADC value of benign and malignant nodule with cutoff value

Test Result Variable(s): ADC value

Area	Std. Error(a)	Asymptotic Sig.(b)	Asymptotic 95% Confidence Interval	
			Lower Bound	Upper Bound
.884	.046	.000	.795	.974

The test result variable(s): VAR00001 has at least one tie between the positive actual state group and the negative actual state group. Statistics may be biased.

a Under the nonparametric assumption

b Null hypothesis: true area = 0.5

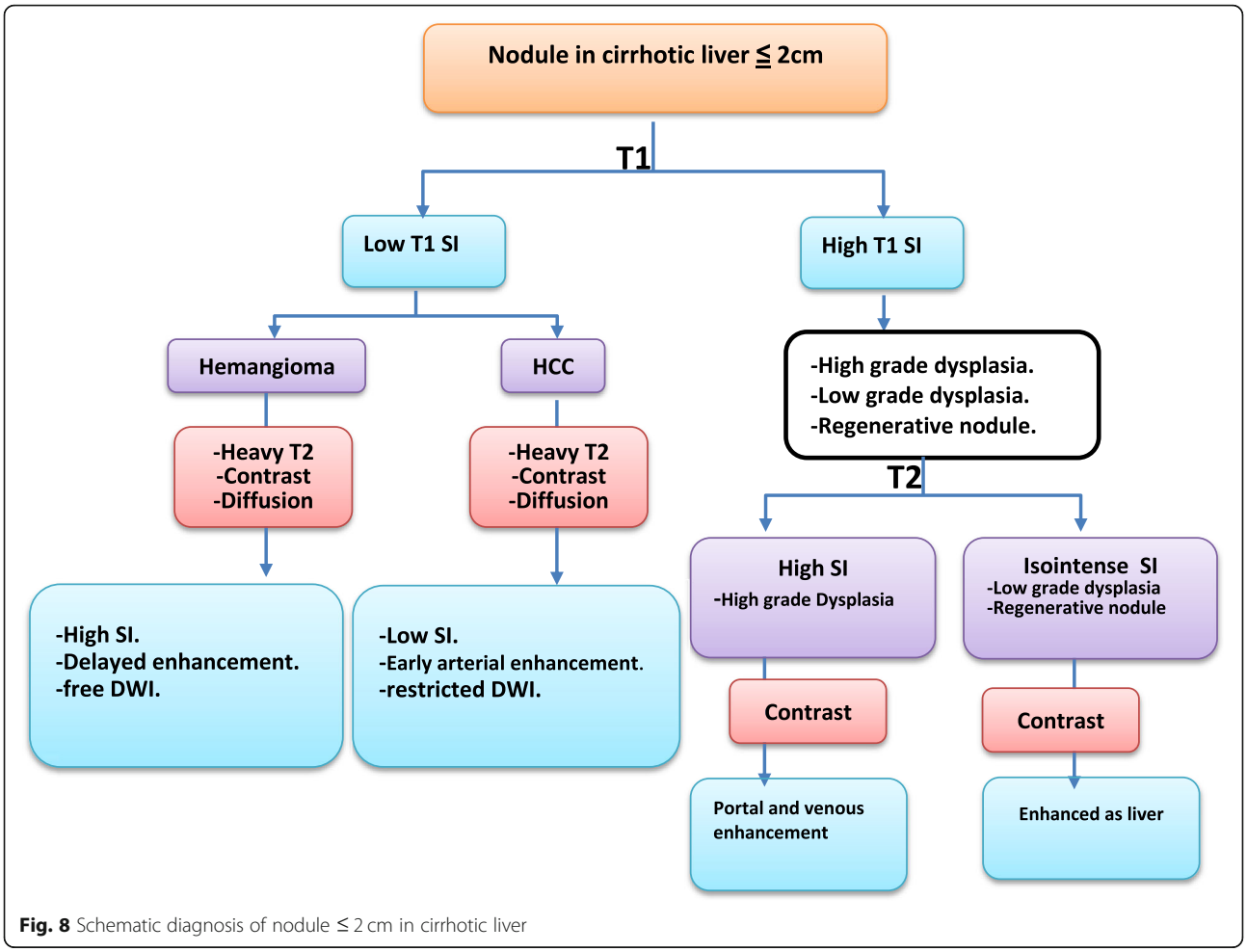

Fig. 8 Schematic diagnosis of nodule ≤ 2 cm in cirrhotic liver

on T1WIs and hyperintense on the T2WIs and SPAIR sequences. In the triphasic study, the nodules showed peripheral nodular enhancement in the arterial phase and no washout in the portal or delayed phase. This finding similar to Debees et al. who studied 5 cases of hemangioma out of 30 cases of hepatic masses on the cirrhotic liver and stated that 4 studied hemangiomas were relatively typical in the appearance and 1 of them appeared with atypical appearance. And they explained this atypical enhancement as hemangioma rarely occurs in end-stage cirrhosis, probably because of the cirrhosis obliterates existing hemangioma.

Our study was done using *b* value of 1000 s/mm^2 for DWIs to overcome the perfusion of the capillary and diffusion of water to the extracellular extravascular space; this high *b* value was needed for reduction of the signal from protons movement in the nearby structure. This will lead to an increase in contrast between the nodule and the liver parenchyma. Moreover, the differentiation between malignant and benign nodules was increased with using high *b* value. This b value was the same that used in studies done by Demir et al. and Hosny [18, 19].

All of group A HCC nodules (72 nodules) and (64/72) nodules (88.8%) had restricted diffusion and 8/72 nodules were partially restricted. This finding was similar to that published by Gaurav et al., who reported that a nodule in the cirrhotic liver with restricted diffusion would be confirmatory to be a malignant nodule, especially when combined with other MRI features of HCC lesions [13]. Mean ADC value of HCCs nodule was $1.40 \times 10^{-3} \pm 0.20 \times 10^{-3}$ mm^2/s.

In our study, dysplastic nodules (28 high grade, 16 low grade) were not restricted with mean ADC value of $1.09 \times 10^{-3} \pm 0.01 \times 10^{-3}$ mm^2/s. Regenerating nodules (8 nodules) showed no restriction with a mean ADC value of $1.2 \times 10^{-3} \pm 0.17 \times 10^{-3}$ mm^2/s. Benign nodules (8 nodules) showed no restriction with a mean ADC of $1.77 \times 10^{-3} \pm 0.35 \times 10^{-3}$ mm^2/s.

Our results are in match with Debees et al. who found an ADC value of HCCs nodule in cirrhotic liver $0.9 \times 10^{-3} \pm 1.3 \times 10^{-3}$ with a mean value of $1.095 \times 10^{-3} \pm$

0.108×10^{-3} and that of regenerating nodules of 1×10^{-3}–1.3×10^{-3} with a mean of $1.98 \times 10^{-3} \pm 0.19 \times 10^{-3}$ and that of hemangioma of $1.8 \times 10^{-3} \pm 2.3 \times 10^{-3}$ with a mean value of $1.98 \times 10^{-3} \pm 0.192 \times 10^{-3}$ and also found the result of ADC statistically significant. Many other studies found significant differences between the ADC value in between benign and malignant nodules but not between various types of malignant lesions or between various types of benign lesions [20–25]. This was matched with our results which succeed in discrimination between benign and malignant nodules with a cutoff value of 1.22×10^{-3} and with a sensitivity of 80% and specificity of 85%.

Other studies by Elbadway et al. found an insignificant difference between the benign and malignant lesions and suggest no definite cutoff value [25].

In our study, we focused on small nodules ≤ 2 cm and found different types of nodules by MRI and confirmed by pathology while Robert et al. stated that lesions with a small diameter were more likely to be benign than malignant [15].

The major limitation of our study was relatively a small number of patients especially those with benign nodules, so future study with much more number of patients is recommended. Also, another limitation was using one kind of contrast medium (Gd-DTPA) to identify different types of nodules. Another promising contrast material is reticuloendothelial agents; these agents are taken by Kupffer cells. Most liver tumors which are deficient in Kupffer cells do not accumulate this agent [25]. And so, liver tumors appear relatively hyperintense as the background liver darkens. This agent are used most routinely to help in the detection of HCC in high risk patients as in the detection of HCC in cirrhotic patients which may be difficult with gadolinium alone, because of several cirrhosis parenchymal changes (fibrosis and regeneration) and alteration of liver perfusion (collaterals, increased hepatic arterial flow relative to portal venous flow) [26]. The use of this agent may help improve HCC detection in such patients when combined with gadolinium to create a double-contrast effect. With this technique, the reticuloendothelial agent was infused first and then followed by gadolinium. The two agents act complementary to improve the contrast of lesion to the liver background on dynamic T1-weighted images because the background liver is darkened by the reticuloendothelial agent while the lesion of interest became more lightened by gadolinium [26, 27]. Further research with newly developed contrast material is recommended.

Conclusion

MRI is promising in differentiating between the different types of small nodules in the cirrhotic liver. This technique can be implemented simply and reliably. It offers the benefit of significantly shorter imaging time, retrospective image reconstruction from the same raw data; it also improves three-dimensional rendering and a high-quality of soft tissue imaging with high intrinsic contrast differentiation of soft tissue. It also provides a global assessment of the abdomen.

Abbreviations

AFP: Alpha-fetoprotein; HCC: Hepatocellular carcinoma; MRI: Magnetic resonance imaging; SI: Signal intensity; US: Ultrasonography; WI: Weighted image

Acknowledgements

Not applicable for this section

Authors' contributions

RA conceived and designed the analysis, collected the data and sample through CT-guided biopsy, performed the data analysis, and wrote the paper. AB performed the pathology study of the collected sample and provided us with the results. Both authors read and approved the final manuscript.

Funding

No funding. Not applicable for this section

Availability of data and materials

The authors confirm that all data supporting the findings of the study are available within the article and the raw data, and data supporting the findings were generated and available at the corresponding author on request.

Ethics approval and consent to participate

The study was approved by the ethical committee of the Faculty of Medicine, Tanta University.

Consent for publication

The authors accepted to publish the paper.

Competing interests

The authors declare that they have no competing of interests.

Author details

[1]Radiology Department, Faculty of Medicine, Tanta University Hospital, Tanta University, 15 Ebn Elphared Street, Tanta, Gharbia Governorate 31511, Egypt. [2]Pathology Department, Faculty of medicine, Tanta University Hospital, Tanta University, Elgesh Street, Tanta, Gharbia Governorate 31511, Egypt.

Received: 10 June 2019 Accepted: 2 July 2019
Published online: 05 August 2019

References

1. Hussain SM, Reinhold C, Mitchell DG (2012) Cirrhosis and lesion characterization at MR imaging. Radiographics 29:1637–1652
2. Hussain SM, Semelka RC, Mitchell DG (2012) MR imaging of hepatocellular carcinoma. Magn Reson Imaging Clin N Am 10:31–52
3. Hanna RF, Aguirre DA, Kased N et al (2014) Cirrhosis associated hepatocellular nodule: correlation of histopathological and MR imaging features. Radiographics 28:747–769
4. Lim JH, Choi D, Cho SK et al (2015) Conspicuity of hepatocellular nodular lesions in cirrhotic livers at ferumoxides-enhanced MR imaging: the importance of Kupffer cell number. Radiology 220:669–676
5. Padaki NR (2014) Nodule in liver: investigations, differential diagnosis, and follow-up. J Clin Exp Hepatol. 4(3):57–62
6. Ishizaki M, Ashida K, Higashi T et al (2014) The formation of capsule and septum in human hepatocellular carcinoma. Virchows Arch 438:574–580
7. Hosny IA (2015) Diffusion MRI of focal liver lesions. Pakistan Journal of Radiology 20:01–07
8. Petra GK, Eric J (2014) Diffusion-weighted imaging in the liver. World J Gastroenterol. 16:1567–1576

9. Glenn GA, Lee VS, Thesis ND et al (2016) Hepatocellular carcinoma and dysplastic nodules in patients with cirrhosis: prospective diagnosis with MR imaging and explanation correlation. Radiology 219:445–454
10. Reieko R, Matsui O, Kobayashi S et al (2015) Cirrhotic nodules: association between MR imaging signal intensity and intranodular blood supply. Radiology 237:512–519
11. Gaurav K, Laura M, Frank HM (2010) MR imaging of hepatocellular carcinoma. Magn Reson Imag Clin North Am 18:421–450
12. Van den bos IC, Hussain SM, Dwarkasing RS et al (2017) MR imaging of hepatocellular carcinoma: the relationship between lesion size and imaging findings, including signal intensity and dynamic enhancement patterns. J Magn Reson Imaging 26:1548–1555
13. Robert J, Tervahartiala P, Isoniemi H et al (2013) Efficacy of sequential use of supra magnetic iron oxide and gadolinium in liver MR imaging. Acta Radiol 43:180–185
14. Jonathan M, Willett HH et al (2016) MR imaging of hepatocellular carcinoma in the cirrhotic liver: challenges and controversies. Radiology 247:311–330
15. Demir OI, Obuz F, Sagol O et al (2016) Contribution of diffusion-weighted MRI to the differential diagnosis of hepatic masses. Diagn Interv Radiol 13:81–86
16. Naglaa LD, Mohamed FS, Gy S (2016) Assessment using dynamic and diffusion-weighted magnetic resonance imaging. Egyptian Journal of Radiology and Nuclear Medicine 47:1221–1230
17. Lowenthal D, Zeile M, Lim WY et al (2011) Detection and characterization of focal liver lesions in colorectal carcinoma patients comparison of diffusion-weighted and Gd-EOB-DTPA enhanced MR imaging. Eur Radiol 21:832–834
18. Tatsuyuki T, Fujimoto K, Qayyum A (2010) Chronic hepatitis and cirrhosis on MR imaging. magnetic resonance imaging. Clinics of North America 18(3):383–402
19. Seale MK, Catalano OA, Saini S et al (2014) Hepatobiliary specific MR contrast agents: role in imaging the liver and biliary tree. Radiographics 29(6):1253–1277
20. Kim T, Murakami T, Takahashi S et al (1999) Diffusion-weighted single-shot echoplanar MR imaging for liver disease. AJR Am J Roentgenol 173:393–398
21. Gourtsoyianni S, Papanikolaou N, Yarmenitis S et al (2008) Respiratory gated diffusion-weighted imaging of the liver: the value of apparent diffusion coefficient measurements in the differentiation between most commonly encountered benign and malignant focal liver lesions. Eur J Radiol 18:486–492
22. Koike N, Cho A, Nasu K et al (2009) Role of diffusion-weighted magnetic resonance imaging in the differential diagnosis of focal hepatic lesions. World J Gastroenterol 15:5805–5812
23. Holzapfel K, Bruegel M, Eiber M et al (2010) Characterization of small (≤10 mm) focal liver lesions: the value of respiratory-triggered echoplanar diffusion-weighted MR imaging. Eur J Radiol 7:89–95
24. Badway NA, Hamisa M (2013) Can diffusion-weighted MR differentiates between benign and malignant hepatic focal lesions. Egyptian J Radiol and Nucl Med 44:453–461
25. Araki T (2000) SPIO-MRI in the detection of hepatocellular carcinoma. J Gastroenterol 35:874–876
26. Ward J, Guthrie JA, Scott DJ et al (2000) Hepatocellular carcinoma in the cirrhotic liver: double-contrast MR imaging for diagnosis. Radiology 216:154–162
27. Bhartia B, Ward J, Guthrie JA, Robinson PJ (2003) Hepatocellular carcinoma in cirrhotic livers: double-contrast thin-section MR imaging with pathologic correlation of explanted tissue. AJR Am J Roentgenol 180:577–584.

Publisher's Note